Simulation-Based Characterization of Mechanical Parameters and Thickness of Homogeneous Plates Using Guided Waves

Michael Ponschab, Daniel A. Kiefer, and Stefan J. Rupitsch, *Member, IEEE*

***Abstract*— Properties of isotropic plates in terms of material constants and thickness are characterized by making use of dispersion characteristics of propagating Lamb waves. A numerical model is inversely optimized in order to match dispersion curves measured by laser vibrometry. This kind of material characterization has gained interest in recent research. Improvements in accuracy and efficiency of the optimization process are therefore important steps toward an industrial application of this technique to nondestructive testing and online monitoring. For this purpose, the use of a fast converging numerical model based on spectral collocation has been found to be well suited. Furthermore, we improved the signal-to-noise ratio by utilizing long-time broadband excitation signals for multimodal excitation of Lamb waves. The wavenumber spectrum up to 2.5 MHz is acquired by measurements with a laser-scanning vibrometer. In order to exploit the information contained in high-order modes, we present an algorithm to match the measured data to the calculated modes during the optimization process, leading to higher accuracy of the estimated model parameters. The characterization results are verified by comparison to measurements with a conventional ultrasonic method.**

***Index Terms*— Guided wave, inverse method (IM), Lamb wave, material characterization, spectral method, ultrasound.**

I. Introduction

An increasing automation of production facilities entails a demand for new ways of online monitoring. The sheet metal working industry relies, therefore, often on radiometric methods or laser-based triangulation in surveillance of the processed materials and to detect defects. Ultrasonic measurement methods provide an attractive alternative and are well established in the field of nondestructive evaluation (NDE) for the characterization of layers and structures [1], as they may not only provide information about the geometry, but also about the material.

Classical ultrasonic techniques utilize time-of-flight measurements with contact transducers to measure the speed of sound or the thickness of plates, while the other size is known [2]. Exploiting reverberation in submerged setups allows for determining both parameters simultaneously [3], [4]. Limitations of axial resolution can be countered if a model-based evaluation of obtained echoes is used [5].

Manuscript received June 18, 2019; accepted August 2, 2019. Date of publication August 7, 2019; date of current version November 21, 2019. This work was financially supported by Diehl Metering. *(Corresponding author: Michael Ponschab.)*

The authors are with the Department of Sensor Technology, Friedrich-Alexander-Universität (FAU), 91052 Erlangen, Germany (e-mail: michael.ponschab@fau.de).

Digital Object Identifier 10.1109/TUFFC.2019.2933699

Other methods are based on the characteristics of guided ultrasonic waves propagating in plates, which are called Lamb waves [6]. As in any waveguide, the propagating waves split into modes of different dispersive wave speeds. These are depicted by so-called dispersion curves, which depend on material constants, plate thickness, and frequency and are therefore suitable to characterize the plate properties. The characterization process depends on time- and space-resolved information on the propagating waves.

Early researchers calculated thickness and isotropic elastic constants from time-domain data [7]–[10] analytically. Later, others used numerical models to inversely characterize Young's modulus by making use of the zero-order Lamb wave modes [11], [12]. For the characterization of orthotropic elastic materials, a method based on image processing making use of high-order modes has been investigated in recent years [13], [14]. With the use of appropriate material models, Bause *et al*. [15] were able to characterize a viscoelastic cylindrical waveguide. An interesting approach, which does not require space-resolved data, is to exploit modes with group velocity tending to zero. Clorennec *et al*. [16] showed how these points of no energy spreading can be exploited by a laser-based measurement to determine the material's bulk velocities. Grünsteidl *et al*. [17] extended the method by modulating the laser spot in order to additionally obtain the plate thickness.

This study aims at improving the aspects of data acquisition, modeling the guided wave problem, and optimization algorithm. Most forenamed authors rely on pulse excitation of Lamb waves. We suggest working with long-time broadband signals instead, as their greater time–bandwidth product leads to a better signal-to-noise ratio [4]. For this purpose, a variable-angle wedge transducer is applied. Together with a reception by laser interferometry with high spatial resolution, this results in sharp distinctive dispersion curves. The high sample rates of the used laser-scanning vibrometer enable the acquisition of high-order Lamb modes. We present an algorithm to sort the extracted measurement data points and the model output to corresponding modes in order to be able to apply a highly effective optimization algorithm for multiple model parameters, while improving the accuracy of the estimated plate parameters. Speeding up the optimization process is an important step toward usage in industrial applications. Modeling the guided wave problem with spectral collocation [18] allows for the calculation of the full Lamb

0885-3010 © 2019 IEEE. Personal use is permitted, but republication/redistribution requires IEEE permission.
See http://www.ieee.org/publications_standards/publications/rights/index.html for more information.

Authorized licensed use limited to: Universitatsbibliothek Erlangen Nurnberg. Downloaded on April 06,2020 at 09:45:45 UTC from IEEE Xplore. Restrictions apply.

Fig. 1. Definition of the coordinate system used for modeling the Lamb wave propagation in the plate.

wave spectrum for 100 frequency points in about 1 s on an average personal computer, due to spectral convergence rates.

This article is organized as follows. The model for the calculation of dispersion characteristics is shown in Section II. Section III deals with the measurement setup used to acquire time- and space-resolved Lamb wave data. In addition, the process of extracting data for plate characterization is explained. The inverse method (IM), fitting the plate model to the measured data, is the content of Section IV. A parameter study reveals the importance of including high-order modes in this process. Results for plates of different thicknesses and materials are discussed in Section V. A conclusion is given in Section VI.

II. Model for Guided Waves

Classically, an analytic model for the propagation of Lamb waves in a plate results from the so-called *characteristic equation* and is found by superimposing reflected partial plane waves from the plate boundaries [6]. As these characteristic equations are transcendental, root-finding algorithms are utilized to obtain dispersion relations. However, the root-finding techniques become cumbersome with more complex problem setups as multiple layers, anisotropy, and open-domain problems such as leaky Lamb waves [19]. The main problem of root-finding algorithms is the possibility of missing solutions due to the utilized mode tracing as well as their extensive calculation time. Nowadays, algorithms avoid these problems by solving the basic differential equations in a numerical way instead of finding roots of the analytical model.

An often-used approach is the semianalytical finite-element (SAFE) method developed by Gavric [20]. Because, in the propagation direction, periodic wave field is assumed, the remaining dimensions are meshed with finite elements, allowing the waveguide to adopt arbitrary cross sections. Plane or cylindrical geometries are modeled along the single dimension of the waveguide's thickness. Especially effective for such simple systems is the use of Chebyshev spectral collocation methods (SCMs), which was first adopted by Adamou and Craster [21] to solve the waveguide problem. Quintanilla *et al.* [22] applied the SCM for calculating anisotropic multi-layer systems. Besides the advantages of finding naturally all eigenvalues and being robust, the SCM additionally converges very fast and is easily implemented in common environments like MATLAB.

For the following mathematical model description, we consider a traction-free homogeneous infinite plate of thickness h. As shown in Fig. 1, the propagation direction of the investigated Lamb waves is aligned with the x-direction, while the finite dimension of the plate thickness is orientated in y-direction. Along the infinite z-direction, homogeneous boundary conditions are considered. Therefore, a plane strain formulation, where the displacements u in x- and y-directions are independent of z, may be used [23]

$$\boldsymbol{u} = [u_{\mathrm{x}}(y), u_{\mathrm{y}}(y), u_{\mathrm{z}}(y)]^{\mathrm{T}} e^{j(k_{\mathrm{x}}x - \omega t)}. \tag{1}$$

The elastic wave propagates harmonically with respect to time t and space according to the angular frequency $\omega = 2\pi f$ and wavenumber k_{x}. A transposition is denoted by $\bullet^{\mathrm{T}}$. Since our measurement setup presented in Section III is only capable of measuring out-of-plane velocities of the plate, solely modes possessing displacements in the y-direction can be captured. For isotropic materials, u_{z} decouples from the other two displacements, which compose the Lamb modes [22]. As only an isotropic material model is used in this article, u_{z} is neglected from now on. We note that the presented model can easily be enhanced in order to deal with anisotropic materials.

The wave propagation inside the plate satisfies Navier's equation of motion (nabla operator ∇, material density ρ)

$$\nabla \cdot [\boldsymbol{\sigma}] = \rho \frac{\partial^2 \boldsymbol{u}}{\partial t^2}. \tag{2}$$

For a linear elastic, isotropic, homogeneous medium, the stresses $\boldsymbol{\sigma}$ are linked with the strains $\boldsymbol{\epsilon}$ by the constitutive equation

$$\begin{bmatrix} \sigma_{\mathrm{xx}} \\ \sigma_{\mathrm{yy}} \\ \sigma_{\mathrm{xy}} \end{bmatrix} = \underbrace{\begin{bmatrix} c_{11} & c_{12} & 0 \\ c_{12} & c_{11} & 0 \\ 0 & 0 & c_{33} \end{bmatrix}}_{\boldsymbol{C}} \begin{bmatrix} \epsilon_{\mathrm{xx}} \\ \epsilon_{\mathrm{yy}} \\ 2\epsilon_{\mathrm{xy}} \end{bmatrix} \tag{3}$$

using Voigt notation and plane strain conditions. The entries of the tensor $\boldsymbol{C}$ can be calculated from the longitudinal and transverse wave speeds c_{l} and c_{t} by $c_{11} = \rho c_{\mathrm{l}}^2$, $c_{12} = \rho(c_{\mathrm{l}}^2 - 2c_{\mathrm{t}}^2)$, and $c_{33} = \rho c_{\mathrm{t}}^2$. The description of the material by wave speeds and density is used here, as the wave speeds are part of the later characterized parameters. With the use of the linear strain–displacement relation $\boldsymbol{\epsilon} = \nabla^{\mathrm{sym}} \boldsymbol{u}$ (symmetric gradient ∇^{sym} [6]), the equation of motion (2) can be written as

$$\nabla \cdot \boldsymbol{C} \cdot \nabla^{\mathrm{sym}} \boldsymbol{u} = \rho \frac{\partial^2 \boldsymbol{u}}{\partial t^2}. \tag{4}$$

Since the plate is assumed to be traction-free, the stresses at the surfaces $y = \pm h/2$ take the form

$$\begin{bmatrix} \sigma_{\mathrm{yy}} \\ \sigma_{\mathrm{xy}} \end{bmatrix}_{y=\pm h/2} = \begin{bmatrix} c_{12} & c_{11} & 0 \\ 0 & 0 & c_{33} \end{bmatrix} \nabla^{\mathrm{sym}} [\boldsymbol{u}]_{y=\pm h/2} = 0. \tag{5}$$

So far, the problem description compromises two second-order differential equations of motion and four boundary conditions, containing continuous functions $\boldsymbol{u}(y)$. These have to be discretized on the problem domain $y \in [-(h/2); (h/2)]$. The SCM makes use of smooth global functions for the approximation of $\boldsymbol{u}(y)$, which is discretized at N points, the so-called collocation points y_i. For a detailed introduction to spectral methods, we refer to Trefethen's book [18] and the MATLAB suite by Weideman and Reddy [24], which we used for our implementation. The SCM offers the advantage of expressing a differentiation by multiplication with a

Authorized licensed use limited to: Universitatsbibliothek Erlangen Nurnberg. Downloaded on April 06,2020 at 09:45:45 UTC from IEEE Xplore. Restrictions apply.

differentiation matrix. For the transition from continuous to discretized variables, the following mappings are applied.

1) Displacements: $\boldsymbol{u} = [u_\mathrm{x}(y), u_\mathrm{y}(y)]^\mathrm{T} \mapsto \underline{u} = [\underline{u}_\mathrm{x}, \underline{u}_\mathrm{y}]^\mathrm{T}$.
2) Differential operators: $\frac{\partial}{\partial y} \mapsto \underline{\underline{D}}_\mathrm{y}$ and $\frac{\partial^2}{\partial y^2} \mapsto \underline{\underline{D}}_\mathrm{yy}$.
3) Constants: $c \mapsto c\underline{\underline{I}}$.

By substituting (1) and (3) and making use of the differentiation matrices $\underline{\underline{D}}_\mathrm{y}$ and $\underline{\underline{D}}_\mathrm{yy}$, each of size $[N \times N]$, and the $[N \times N]$-sized identity matrix $\underline{\underline{I}}$, the equation of motion (4) reads as

$$\overbrace{\begin{bmatrix} -k_\mathrm{x}^2 c_{11}\underline{\underline{I}} + c_{33}\underline{\underline{D}}_\mathrm{yy} & jk_\mathrm{x}(c_{12}+c_{33})\underline{\underline{D}}_\mathrm{y} \\ jk_\mathrm{x}(c_{12}+c_{33})\underline{\underline{D}}_\mathrm{y} & -k_\mathrm{x}^2 c_{33}\underline{\underline{I}} + c_{11}\underline{\underline{D}}_\mathrm{yy} \end{bmatrix}}^{\underline{\underline{L}}_{2N\times 2N}} \underline{u} = \omega^2 \underbrace{\begin{bmatrix} -\rho\underline{\underline{I}} & 0 \\ 0 & -\rho\underline{\underline{I}} \end{bmatrix}}_{\underline{\underline{M}}_{2N\times 2N}} \underline{u}. \tag{6}$$

The stresses for the boundary equation (5) take the form

$$\underbrace{\begin{bmatrix} jk_\mathrm{x}c_{12}\underline{\underline{I}} & c_{11}\underline{\underline{D}}_\mathrm{y} \\ c_{33}\underline{\underline{D}}_\mathrm{y} & jk_\mathrm{x}c_{33}\underline{\underline{I}} \end{bmatrix}}_{\underline{\underline{S}}_{2N\times 2N}} \underline{u} = 0. \tag{7}$$

Each row of the system of equations (6) represents the displacement at one collocation point. The lines $1, N, N+1$, and $2N$ define the displacement at the borders. The boundary conditions are taken into account by replacing those lines of L in (6) by the corresponding ones of S from (7) and the lines of M by 0. The resulting system of the form

$$\underline{\underline{A}}\,\underline{u} = \omega^2 \underline{\underline{B}}\,\underline{u} \tag{8}$$

represents a general eigenvalue problem and can be solved by inserting wavenumbers and computing the corresponding angular frequencies. To calculate k_x for a given frequency, the dependence of $\underline{\underline{A}}$ on k_x in (8) is written as a quadratic eigenvalue problem of the form

$$k_\mathrm{x}^2\underline{\underline{A}}_2 + k_\mathrm{x}\underline{\underline{A}}_1 + (\underline{\underline{A}}_0 - \omega^2\underline{\underline{B}}) = 0 \tag{9}$$

by sorting the terms in $\underline{\underline{A}}$ by power of k_x into separate matrices $\underline{\underline{A}}_2$,$\underline{\underline{A}}_1$, and $\underline{\underline{A}}_0$. For both problems (8) and (9), effective solving routines exist. This allows calculating the complete model $m(f, c_\mathrm{l}, c_\mathrm{t}, \rho, h) \mapsto k_\mathrm{x}(f)$ with sufficient precision in a few seconds. Therefore, the described model is well suited for the purpose of fast inverse material characterization.

III. Data Acquisition

The acquisition of frequency-dependent wavenumbers requires measurement of space- and time-dependent Lamb wave data. In this section, we first explain our measurement setup, followed by a presentation of the processing used to retrieve the measured wavenumbers.

A. Measurement Setup

For the measurement of dispersion data, different setups are possible. Generally, one could distinguish between contact [25], [26] and noncontact excitation [25], [14] as well as between contact [14], [26] and noncontact reception of Lamb waves [8], [27]. We chose a contact excitation with a variable-angle beam transducer as depicted in Fig. 2. The used longitudinal wave transducer (C401, Olympus Inc., Waltham, MA, USA) features a center frequency of 1.1 MHz and 88% fractural bandwidth. As the excitation of Lamb waves by means of angle beam transducers follows Snell's law, Lamb wave modes with phase velocities of $c_\mathrm{p} = c_\mathrm{w}/\sin\theta_\mathrm{i}$ will mainly be excited [2]. Herein, c_w corresponds to the longitudinal wave speed of the acrylic glass wedge and θ_i to the incidence angle. Since it is desirable to have a wide range of phase velocities available for the material characterization, the ability to adjust the beam angle is advantageous. During the measurements, it was observed that the use of four incident angles at 10°, 20°, 40°, and 70° is sufficient because the directivity pattern of the ultrasound transducer leads to a larger range of exciting phase velocities as shown in Fig. 3. The transducer was placed on an aluminum EN AW-5754 plate with 2-mm thickness. All experiments were conducted with a glycerin coupling. Therefore, mainly normal stresses were transmitted from the transducer to the test plate. For the excitation of the ultrasound transducer, we utilized an arbitrary function generator, Keysight 33220A, together with a

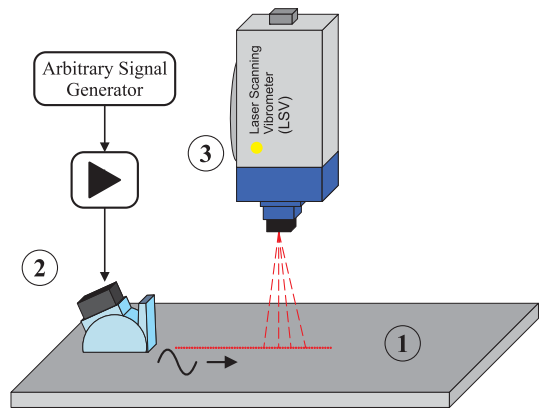

Fig. 2. Sketch of the measurement setup containing a plate-shaped test specimen (1), a variable-angle transducer (2) for the excitation, and a laser-scanning vibrometer (3) for the reception of Lamb waves.

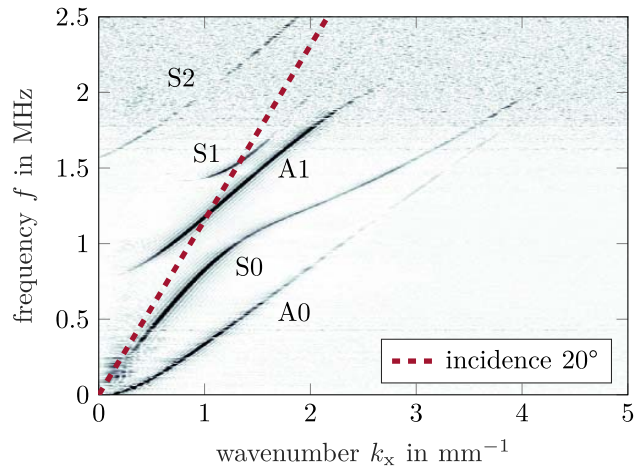

Fig. 3. Dispersion curves acquired by applying a 2-D-FFT to measurement data from an aluminum plate with 2-mm thickness. Here, an incidence angle of 20° has been used.

Authorized licensed use limited to: Universitatsbibliothek Erlangen Nurnberg. Downloaded on April 06,2020 at 09:45:45 UTC from IEEE Xplore. Restrictions apply.

high-speed power amplifier (4005, NF Electronic Instruments, Yokohama, Japan).

The time-dependent normal surface velocities of propagating Lamb waves were measured by a laser-scanning vibrometer (PSV-500, Polytec GmbH, Waldbronn, Germany). A line of 389 measurement points with a sampling interval of 0.35 mm was defined, which theoretically allows for the acquisition of wavenumbers up to 17.95 mm^{-1} due to the Nyquist theorem. The measured time signals were sampled with a rate of 12.5 MHz over the duration of 200 μs. Each recording was triggered by the function generator. For the reduction of noise, the time signals of each measurement point were averaged 100 times at a repetition rate of 100 Hz.

The applied excitation signal was designed to cover the whole transducer bandwidth in order to maximize the received frequency information. Other research studies rely on pulsed excitation for this purpose. A disadvantage of such excitation is that the signal-to-noise ratio may only be increased by higher excitation amplitudes, which is technically limited. Coded signals can be used instead to circumvent this limitation [4]. These phase- or frequency-modulated signals provide a greater time–bandwidth product, which improves the signal-to-noise ratio. For our purpose, excitation with a pseudo-random sequence produced good results. Alternatively, chirp signals could also be considered. The used arbitrary signal consists of normally distributed zero mean values, which were sampled at 5 MHz, and features a total duration of 0.1 ms. The same signal sequence was used during the whole measurement.

B. Processing

The shown measurements contain sampled time- and space-dependent information about propagating Lamb modes. Because of the chosen excitation, the modes are superimposed and they cannot be separated in the time domain. With a view to tackling this problem, Alleyne and Cawley [25] suggested using a 2-D fast Fourier transform (2-D-FFT) on signals measured with two angle beam transducers, while one transducer was moved in the propagation direction. As a result of discrete signal processing, leakage may occur, if the time and spatial signals are not periodic within the sampling windows. Therefore, we applied window functions in time and space to reduce this effect. Here, a Tukey window is used for this purpose. For a finer resolution of the dispersion data, zero padding is used before performing the 2-D-FFT.

Fig. 3 shows the color-coded amplitudes of the 2-D Fourier-transformed measurement data for excitation with an incidence angle of 20°. The dashed line depicts the theoretical excited wavenumbers for this angle and frequencies. Naturally, the Lamb modes are best excited in this area, which are illustrated by deep dark lines. Also, the two fundamental modes, as well as the S_2 mode, are already visible.

For the extraction of test data, a peak search is utilized. For each row, a point on the dispersion curves is defined according to two conditions: 1) a peak must be at least five times as high as the mean value of this row and 2) a minimum distance of 200 m^{-1} between two peaks is prescribed under the assumption that no mode crossings occur in this frequency region. The resulting data points are displayed in Fig. 4.

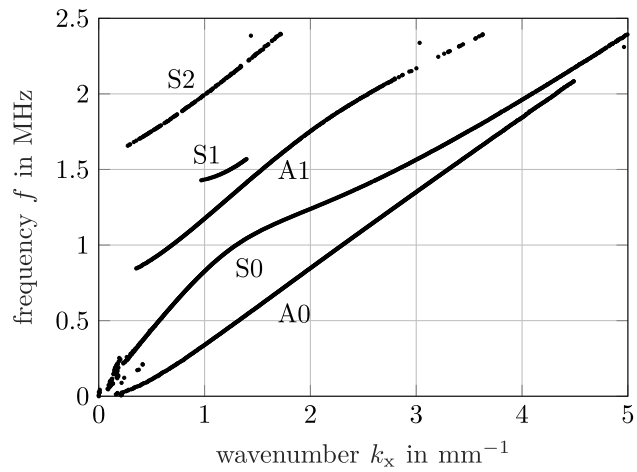

Fig. 4. Extracted measurement points from 2-D-FFT data as shown in Fig. 3 from measurements with multiple incidence angles.

All modes propagating below 2.5 MHz, except the S_1 mode, have been captured. Large wavelengths seem to be difficult to measure with this setup, which results in noisy data for the S_0 mode at small wavenumbers. These are cut off for the inverse material characterization.

IV. Inverse Method

A convenient way to match measured data with a mathematical model is by the application of an IM. The basic principle of this method is to iteratively adjust a set of input parameters in order to match the model to the test data as best as possible. From a mathematical point of view, an inverse problem is the opposite of a direct problem, which refers to a mapping $A\colon X \to Y$ of causes $x \in X$ onto the effects $y \in Y$ [28]. For all causes x, an effect $y = Ax$ can be found. The inverse problem of finding the causes $x = A^{-1}y$ from measured effects is a recurring topic for the estimation of system parameters and material properties. Unfortunately, this problem is generally an ill-posed one because the possible solutions are not necessarily unique and, more importantly, the inverse mapping is often not stable due to measurement errors and model incorrectness [23]. Therefore, regularization techniques, as well as iterative corrections, are indispensable in order to transform the ill-posed problem to a neighboring well-posed one, which is suitable for finding the correct causes x [28].

A. Parameter Study

The IM is a tool to determine a set of parameters based on information contained in model and measurement data. It fails to estimate the correct parameters when no or not enough information is available. In order to investigate, if the used Lamb wave dispersion data are satisfactory for the determination of the target parameters c_l, c_t, and h, a parameter study is consulted. The numerical model is used to calculate a set of dispersion curves depicted in Fig. 5. For each figure, one parameter is altered in the range $\pm 10\%$ around the default values for aluminum and a thickness of 2 mm, while the others are kept constant. Modes showing greater variations due to certain parameter changes deliver a more valuable contribution to the estimation of that parameter.

Authorized licensed use limited to: Universitatsbibliothek Erlangen Nurnberg. Downloaded on April 06,2020 at 09:45:45 UTC from IEEE Xplore. Restrictions apply.

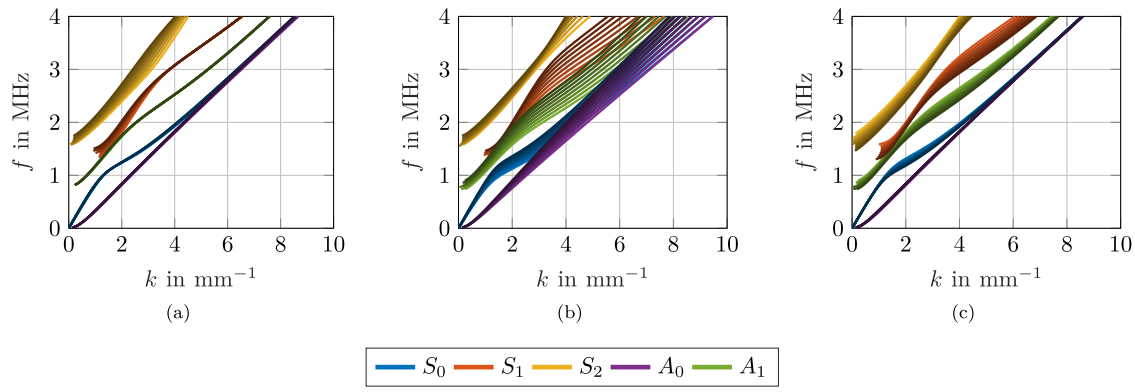

Fig. 5. Parameter study on the influence of the searched parameters on the dispersion data. c_{l} is modified in (a) and all other parameters are kept constant. The same procedure is used in (b) and (c) for c_{t} and h, respectively. Information on the variation of $+10\%$ (dark) to -10% (bright) is provided by shading while different Lamb modes are color coded. (a) Modification of c_{l}. (b) Modification of c_{t}. (c) Modification of h.

An important observation made from Fig. 5(a) is that the longitudinal wave speed c_{l} has only little influence on the fundamental modes as well as the first antisymmetric mode. Subsequently, an estimation of this parameter will be afflicted with errors, if solely information on these modes is available for material characterization. The greater impact of c_{l} on the higher symmetric modes makes a reliable estimation still possible. With increasing frequency, the fundamental modes converge to the Rayleigh wave speed c_R, which is approximative linear proportional to c_{t} [29], while the higher modes converge to c_{t} [2]. Accordingly, the impact of c_{t} on k_{x} increases with increasing frequency, which is also indicated by Fig. 5(b). A normalized plot of fh over $k_{\mathrm{x}}h$ is dimensionless and is therefore independent on the thickness h. The parameter h leads consequently to a shift of the dispersion curves along a diagonal line. As a conclusion, it could be stated that all three parameters can be identified simultaneously if the measurement data on the higher symmetric modes exist.

B. Implementation

For the approximation of the searched parameters $\boldsymbol{p} = [c_{\mathrm{l}}, c_{\mathrm{t}}, h]^{\mathrm{T}}$, we use an iteratively regularized Gauss–Newton algorithm, which has already been found suitable for the characterization of piezoelectric materials [30]. This algorithm is based on a Tikhonov function and converges quickly to a solution while staying stable.

The measured test data $\boldsymbol{q}_{\mathrm{m}}$ as well as the simulated quantities $\boldsymbol{q}_{\mathrm{s}}(\boldsymbol{p})$, each representing the wavenumbers k_{x}, are gathered in equally sized vectors. During the characterization process, minimization of their quadratic deviation given by

$$\min_{\boldsymbol{p}} \Psi(\boldsymbol{p}) = \min_{\boldsymbol{p}} \|\boldsymbol{q}_{\mathrm{s}}(\boldsymbol{p}) - \boldsymbol{q}_{\mathrm{m}}\|_2^2 \tag{10}$$

is performed by a Gauss–Newton method, approaching the minimum with each step i. The parameter vector is adjusted stepwise by

$$\boldsymbol{p}^{(i+1)} = \boldsymbol{p}^{(i)} + \boldsymbol{c}^{(i)} \tag{11}$$

and the necessary correction for this algorithm is given by [28]

$$\boldsymbol{c}^{(i)} = -\left[\boldsymbol{J}(\boldsymbol{p}^{(i)})^{\mathrm{T}}\boldsymbol{J}(\boldsymbol{p}^{(i)}) + \zeta_{\mathrm{R}}^{(i)}\boldsymbol{I}\right]^{-1} \cdot\left[\boldsymbol{J}(\boldsymbol{p}^{(i)})^{\mathrm{T}}\boldsymbol{d}_{\mathrm{I}}(\boldsymbol{p}^{(i)}) + \zeta_{\mathrm{R}}^{(i)}(\boldsymbol{p}^{(i)} - \boldsymbol{p}^{(0)})\right]. \tag{12}$$

Hereby, $\boldsymbol{I}$ is the identity matrix. The parameter correction $\boldsymbol{c}^{(i)}$ depends on the deviation of the measured and simulated quantities

$$\boldsymbol{d}_{\mathrm{I}}(\boldsymbol{p}^{(i)}) = \boldsymbol{q}_{\mathrm{s}}(\boldsymbol{p}) - \boldsymbol{q}_{\mathrm{m}} \tag{13}$$

and its first-order derivative

$$\boldsymbol{J}(\boldsymbol{p}^{(i)}) = \left.\frac{\partial \boldsymbol{d}_{\mathrm{I}}(\boldsymbol{p}^{(i)})}{\partial \boldsymbol{p}}\right|_{\boldsymbol{p}=\boldsymbol{p}^{(i)}} = \left.\frac{\partial \boldsymbol{q}_{\mathrm{s}}(\boldsymbol{p}^{(i)})}{\partial \boldsymbol{p}}\right|_{\boldsymbol{p}=\boldsymbol{p}^{(i)}}. \tag{14}$$

Furthermore, we exploit Tikhonov regularization to stabilize an oscillating $\boldsymbol{p}$. The regularization parameter $\zeta_R^{(i)}$ is reduced according to $\zeta_{\mathrm{R}}^{(i)} = 0.8\zeta_{\mathrm{R}}^{(i-1)}$. For a more detailed description of the used algorithm, one may refer to [28].

In most applications of IMs on material characterization, the model design and the large number of parameters present the most challenging tasks. In our case, building of appropriate quantity vectors of wavenumbers from simulation $\boldsymbol{k}_{\mathrm{s}}$ and measurement $\boldsymbol{k}_{\mathrm{m}}$ pose greater difficulties. These wavenumbers are provided as matrices

$$[\boldsymbol{k}] = \left[\begin{array}{c} \xrightarrow{\quad\text{modes}\quad} \\ \text{frequencies}\downarrow \end{array}\right]$$

with sizes $N_{\mathrm{f}} \times N_{\mathrm{s}}$ and $N_{\mathrm{f}} \times N_{\mathrm{m}}$, where N_{f} is related to the sampled frequencies and the second dimension accumulates the wavenumbers of all modes found at this frequencies for simulation and measurement, respectively. In general, $N_{\mathrm{m}} \neq N_{\mathrm{s}}$. Because higher modes only occur for frequencies above their cutoff frequency, the matrices are not fully populated.

In principle, it is desired to arrange the wavenumbers that are sampled along a range of frequencies and related to a number of modes in a vector

$$\boldsymbol{q} = \begin{bmatrix} \boldsymbol{k}_{\mathrm{S0}}^{\mathrm{T}} & \text{for } f_0^{\mathrm{S1}}, \ldots, f_N \\ \boldsymbol{k}_{\mathrm{S2}}^{\mathrm{T}} & \text{for } f_0^{\mathrm{S0}}, \ldots, f_N \\ \boldsymbol{k}_{\mathrm{S1}}^{\mathrm{T}} & \text{for } f_0^{\mathrm{S2}}, \ldots, f_N \\ \boldsymbol{k}_{\mathrm{A0}}^{\mathrm{T}} & \text{for } f_0^{\mathrm{A0}}, \ldots, f_N \\ \boldsymbol{k}_{\mathrm{A1}}^{\mathrm{T}} & \text{for } f_0^{\mathrm{A1}}, \ldots, f_N \end{bmatrix}. \tag{15}$$

Authorized licensed use limited to: Universitatsbibliothek Erlangen Nurnberg. Downloaded on April 06,2020 at 09:45:45 UTC from IEEE Xplore. Restrictions apply.

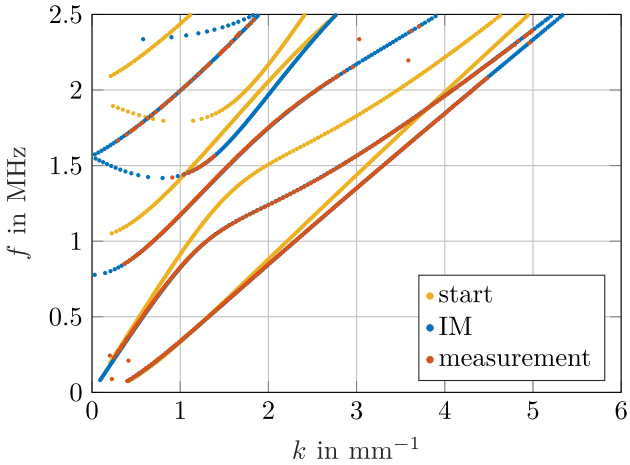

Fig. 6. Results for the characterization of the properties of a 2-mm aluminum plate. The calculated dispersion curves with initial parameters $\boldsymbol{p}^{(0)}$ are deviated about 10% around values from the literature. The results calculated by parameter characterization (blue) match perfectly with the measurement data (red).

This task could easily be done for the simulated data due to the knowledge of the corresponding displacement fields along the plate thickness and by sorting the wavenumbers by size. However, sorting the measurement data according to (15) is troublesome as the necessary information about the displacement fields is not available for the measurement data. In addition, the data acquisition is imperfect and, consequently, parts of the dispersion curves might be missing, as shown in Fig. 4. Pure sorting of the modes by wavenumber magnitude will, therefore, be afflicted with errors.

An approach to solve this problem is to sort the simulated and measured wavenumbers according to nearest neighbors. The underlying procedure can be summarized as follows.

1) Calculate $\boldsymbol{k}_\mathrm{s}$ by evaluating the model for N_f frequencies $\boldsymbol{f}$, at which $\boldsymbol{k}_\mathrm{m}$ has been sampled.
2) Iterate over occupied entries of $\boldsymbol{k}_\mathrm{m}$ with index $i \in [1, N_\mathrm{f}]$, $j \in [1, N_\mathrm{m}]$, and $\boldsymbol{q}_\mathrm{s}, \boldsymbol{q}_\mathrm{m}$ with index $n = ij$.
3) For each single $k_\mathrm{m}^{(i,j)}$ and each row $\boldsymbol{k}_s^{(i)}$, find $\Delta k^{(p)} = \min_{p\in[1,N_\mathrm{s}]} |k_\mathrm{s}^{(i,p)} - k_\mathrm{m}^{(i,j)}|$.
4) If there is a $\Delta k^{(p)} < \delta$, i.e., smaller than a threshold δ, assign $q_\mathrm{s}^{(n)} = k_\mathrm{s}^{(i,p)}$ and $q_\mathrm{m}^{(n)} = k_\mathrm{m}^{(i,j)}$. Otherwise, skip entry $k_\mathrm{m}^{(i,j)}$.

This can be used to build the test data q_m and a map used to transform the model data to q_s during each iteration step. Defining a threshold δ assures that only pairs $k_\mathrm{s}^{(l)}$ and $k_\mathrm{m}^{(j)}$ are considered for the algorithm, which likely refers to the same mode. Handling the quantities in this manner will work well if the initial guess $\boldsymbol{p}^{(0)}$ deviates marginally from the real parameter vector. However, if the divergences are greater than a few percent, two effects observable, for instance, in Fig. 6 might prevent a successful material characterization: 1) the cutoff frequencies of higher modes can lead to situations during the iteration where the mapping of $\boldsymbol{q}_\mathrm{s}$ results in unallocated entries and 2) interceptions of different measured and simulated modes occur, which are interpreted as fitting data points.

As a solution, we suggest to adjust $\boldsymbol{q}_\mathrm{m}$ and $\boldsymbol{q}_\mathrm{s}$ according to the described procedure at each iteration step. Therefore, the forenamed first problem can be avoided as the mapping is done for each $\boldsymbol{k}_\mathrm{s}^{(i)}$ separately. The mapping of wrong $(k_\mathrm{s}, k_\mathrm{m})$ pairs will still occur, but happens less for later iteration steps, if enough true $(k_\mathrm{s}, k_\mathrm{m})$ pairs exist that result in the right $\boldsymbol{p}$. An additional advantage of an iterative mapping is that the threshold δ can be slightly reduced for each step i in the same manner as ζ_R according to $\delta^{(i+1)} = 0.95\delta^{(i)}$, ensuring a neglect of false data points due to noise at later iteration steps.

Tests with simulated and measured data yield best results with a regularization $\zeta_\mathrm{R}^{(0)} = 10^3$ and a threshold $\delta^{(0)} = 180\ \mathrm{m}^{-1}$. Material parameter values provided by the manufacturer, which were altered randomly in the range of $\pm 10\%$, are used as initial guess $\boldsymbol{p}^{(0)}$. Because of the huge difference in the scale of wave speeds and plate thickness, $\boldsymbol{p}^{(0)}$ is normalized prior to characterization. Convergence is defined to be reached if $\|\boldsymbol{d}^{(i)}/\boldsymbol{p}^{(i)}\| < 10^{-5}$. Using measurement data with about 2000 frequency points, the algorithm converges in approximately 10 iteration steps. The calculation takes about 4 min on an average PC (Intel Core i5-6600, 16-GB RAM).

V. Results

With a view of testing the stability of the proposed parameter characterization, we applied the identification procedure on the simulated as well as the measured data. Fig. 6 shows the results for the data provided in Figs. 3 and 4. The yellow dotted lines show the model output for significantly altered initial guess $\boldsymbol{p}^{(0)}$. The agreement between the resulting blue dotted curves and the measured orange dotted curves proves that the algorithm still converges to the correct parameters. We repeated the calculation with randomly changed start parameters, which converged in most cases. All converged cases led to the same set of parameters.

We performed reference measurements to verify the obtained parameters. A micrometer screw gauge was used to measure the plate thickness. The accuracy of the gauge is 0.02 mm. The average of four thickness measurements at different positions was taken as reference. Standard time-of-flight measurements with contact transducers were conducted in order to measure the wavespeeds. Longitudinal and shear waves were excited with an Olympus V112 transducer (center frequency of 10 MHz) and an Olympus V156 transducer (center frequency of 5 MHz), respectively. A pulser-receiver (Panametrics-NDT 5900) was utilized for excitation and reception.

The parameter characterization and reference measurements were conducted with four samples: three aluminum plates of 1, 2, and 3 mm thicknesses and a 1 mm brass plate. Table I lists the obtained values of c_l, c_t, and h and the relative deviation in percent related to the reference measurements in parentheses. These deviations depend on the errors of the reference measurement combined with the errors of our proposed method. The sources for errors of the parameter characterization are identified to depend mainly on the quality of the measurement point coordinates. The measurement device reported a precision of 0.1 mm during calibration.

Authorized licensed use limited to: Universitatsbibliothek Erlangen Nurnberg. Downloaded on April 06,2020 at 09:45:45 UTC from IEEE Xplore. Restrictions apply.

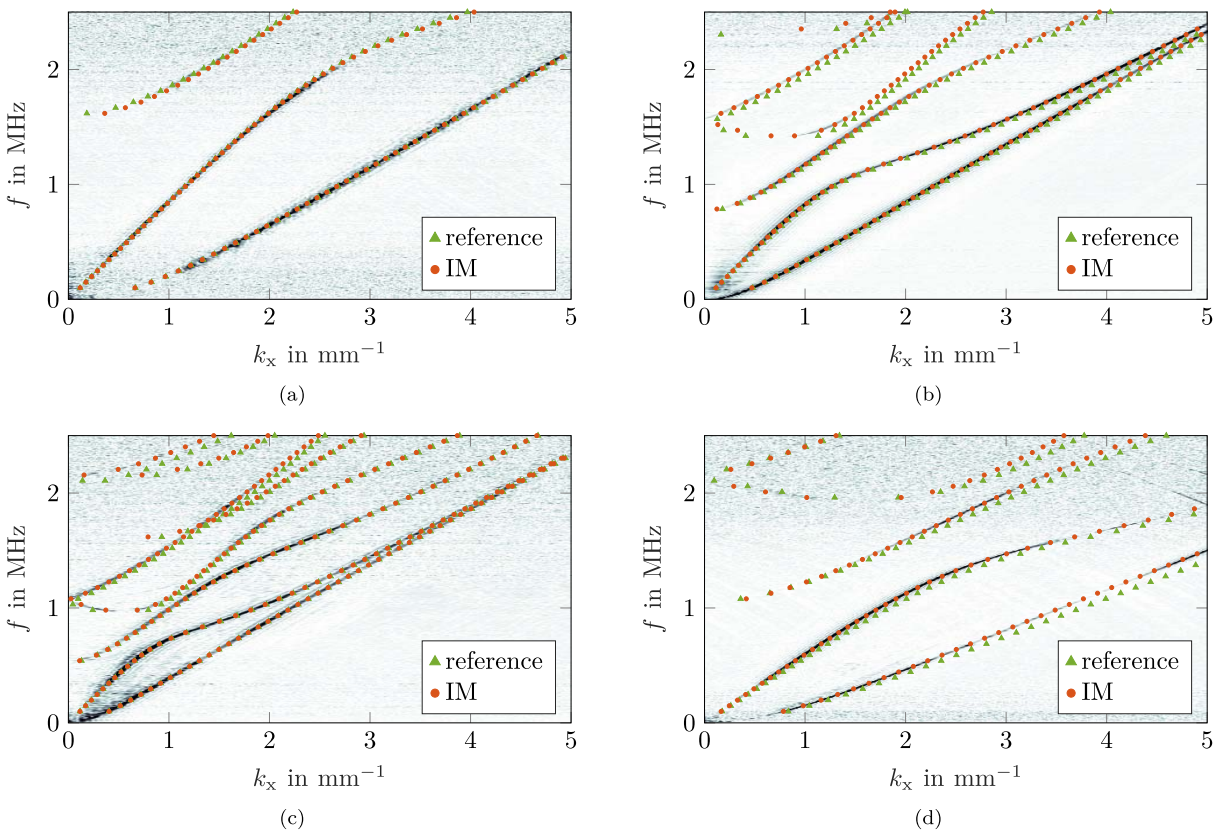

Fig. 7. Results for (a) 1, (b) 2, and (c) 3 mm aluminum and (d) 1 mm brass samples. The sparse dotted curves, plotted over the measured dispersion data, present the model output for parameters obtained by the IM and reference measurement, respectively.

TABLE I

COMPARISON OF PARAMETERS ATTAINED BY CHARACTERIZATION (IM) AND REFERENCE MEASUREMENT; DEVIATION IN % IN PARENTHESES RELATE TO THE REFERENCE MEASUREMENTS

Sample		Parameter		
		c_l(mm/s)	c_t(mm/s)	h(mm)
aluminium 1 mm	IM	6.07(–)	3.14(5.4 %)	0.99(2.2 %)
	ref.	–	3.12	0.97
aluminium 2 mm	IM	6.41(2.0 %)	3.18(1.9 %)	2.05(0.7 %)
	ref.	6.29	3.12	2.03
aluminium 3 mm	IM	6.39(1.4 %)	3.15(0.1 %)	2.97(−0.6 %)
	ref.	6.31	3.15	2.98
brass 1 mm	IM	4.50(6.4 %)	2.17(5.4 %)	1.04(6.8 %)
	ref.	4.23	2.05	0.97

Additional errors were introduced by noise due to low laser signals because of no or nondiffuse reflection.

It is noted that a higher stability, allowing a greater deviation of the initial parameters, can be observed, if fewer modes are used for the identification process. The reason is the rare false intersection of modes. On the other hand, the parameter precision will increase, if more modes and, therefore, more data are available, as shown in Fig. 7(c).

As predicted from the parameter study in Section IV-A, the longitudinal wave speed is mostly afflicted with the highest deviation. Still, all errors stay in the range of a few percent and agree well with the reference measurements. Remarkably, it is even possible to determine a reasonable c_l for the 1-mm aluminum sample with a 1 MHz centered excitation in contrast to the 10 MHz reference measurement. As the deviation decreases with increasing plate thickness [compare Fig. 7(c)], we attribute the deviation mainly to the reference measurements.

VI. CONCLUSION

The determination of elastic material constants and the simultaneous determination of wave speed and thickness are well-studied problems. The benefit of this work becomes apparent in providing a one-sided technique of simultaneously estimating material constants and thickness of plates. This method is based on optical measurements of Lamb waves and determining the parameters with an IM based on fast modeling of the dispersive Lamb wave modes.

The described numerical model of elastic waves in plates based on spectral collocation can easily be implemented and calculates the dispersive Lamb wave modes efficiently. The shown measurement system containing a laser vibrometer produces clear information on the Lamb wave modes. After processing the data, frequency-dependent wavenumbers could be retained. On the basis of this, an easy-to-implement, stable, and fast IM algorithm estimates the desired plate properties. We presented results for four samples of different thicknesses and materials. The estimated parameters agree very well with reference measurements. It could be observed that the quality of the parameter estimation increases with thicker plates since more Lamb modes occur. The same effect can be reached by using higher frequencies.

Authorized licensed use limited to: Universitatsbibliothek Erlangen Nurnberg. Downloaded on April 06,2020 at 09:45:45 UTC from IEEE Xplore. Restrictions apply.

Further investigations on the noncontact characterization of anisotropic materials as well as third-order elastic constants could be contemplated for future work. Moreover, the exchange of the Lamb wave excitation technique toward a laser-based noncontact excitation, as presented by other authors, results in a noncontact measurement device, which may be worth considering in industrial usage for product monitoring.

References

[1] T. Kundu, *Ultrasonic and Electromagnetic NDE for Structure and Material Characterization: Engineering and Biomedical Applications*. Hoboken, NJ, USA: CRC Press, 2012.

[2] J. L. Rose, *Ultrasonic Waves in Solid Media*, 1st ed. Cambridge, U.K.: Cambridge Univ. Press, 2014.

[3] D. K. Hsu and M. S. Hughes, "Simultaneous ultrasonic velocity and sample thickness measurement and application in composites," *J. Acoust. Soc. Amer.*, vol. 92, no. 2, pp. 669–675, Aug. 1992.

[4] D. A. Kiefer, M. Fink, and S. J. Rupitsch, "Simultaneous ultrasonic measurement of thickness and speed of sound in elastic plates using coded excitation signals," *IEEE Trans. Ultrason., Ferroelectr., Freq. Control*, vol. 64, no. 11, pp. 1744–1757, Nov. 2017.

[5] X. Bai, Z. Sun, J. Chen, and B.-F. Ju, "A novel technique for the measurement of the acoustic properties of a thin linear-viscoelastic layer using a planar ultrasonic transducer," *Meas. Sci. Technol.*, vol. 24, no. 12, 2013, Art. no. 125602.

[6] B. A. Auld, *Acoustic Fields and Waves in Solids*, 2nd ed. Melbourne, FL, USA: Krieger, 1990.

[7] R. J. Dewhurst, C. Edwards, A. D. W. McKie, and S. B. Palmer, "Estimation of the thickness of thin metal sheet using laser generated ultrasound," *Appl. Phys. Lett.*, vol. 51, no. 14, pp. 1066–1068, 1987.

[8] D. A. Hutchins, K. Lundgren, and S. B. Palmer, "A laser study of transient Lamb waves in thin materials," *J. Acoust. Soc. Amer.*, vol. 85, no. 4, pp. 1441–1448, 1989.

[9] W. P. Rogers, "Elastic property measurement using Rayleigh–Lamb waves," *Res. Nondestruct. Eval.*, vol. 6, no. 1, pp. 185–208, 1995.

[10] W. Gao, C. Glorieux, and J. Thoen, "Laser ultrasonic study of Lamb waves: Determination of the thickness and velocities of a thin plate," *Int. J. Eng. Sci.*, vol. 41, no. 2, pp. 219–228, 2003.

[11] M. Sale, P. Rizzo, and A. Marzani, "Semi-analytical formulation for the guided waves-based reconstruction of elastic moduli," *Mech. Syst. Signal Process.*, vol. 25, no. 6, pp. 2241–2256, 2011.

[12] L. Ambrozinski, P. Packo, L. Pieczonka, T. Stepinski, T. Uhl, and W. J. Staszewski, "Identification of material properties—Efficient modelling approach based on guided wave propagation and spatial multiple signal classification," *Struct. Control Health Monitor.*, vol. 22, no. 7, pp. 969–983, 2015.

[13] S. Johannesmann, J. Düchting, M. Webersen, L. Claes, and B. Henning, "An acoustic waveguide-based approach to the complete characterisation of linear elastic, orthotropic material behaviour," *Technisches Messen*, vol. 85, nos. 7–8, pp. 478–486, 2018.

[14] M. Webersen, S. Johannesmann, J. Düchting, L. Claes, and B. Henning, "Guided ultrasonic waves for determining effective orthotropic material parameters of continuous-fiber reinforced thermoplastic plates," *Ultrasonics*, vol. 84, pp. 53–62, Mar. 2018.

[15] F. Bause, B. Henning, B. Huang, and A. Kunoth, "Ultrasonic waveguide signal decomposition using the synchrosqueezed wavelet transform for modal group delay computation," in *Proc. IEEE Int. Ultrason. Symp. (IUS)*, Jul. 2013, pp. 671–674.

[16] D. Clorennec, C. Prada, and D. Royer, "Local and noncontact measurements of bulk acoustic wave velocities in thin isotropic plates and shells using zero group velocity Lamb modes," *J. Appl. Phys.*, vol. 101, no. 3, 2007, Art. no. 034908.

[17] C. Grünsteidl, T. Berer, M. Hettich, and I. Veres, "Determination of thickness and bulk sound velocities of isotropic plates using zero-group-velocity Lamb waves," *Appl. Phys. Lett.*, vol. 112, no. 25, 2018, Art. no. 251905.

[18] L. N. Trefethen, *Spectral Methods in MATLAB* (Software, Environments, Tools), 3rd ed. Philadelphia, PA, USA: SIAM, 2008.

[19] D. A. Kiefer, M. Ponschab, S. J. Rupitsch, and M. Mayle, "Calculating the full leaky Lamb wave spectrum with exact fluid interaction," *J. Acoust. Soc. Amer.*, vol. 145, no. 6, p. 3341, 2019.

[20] L. Gavrić, "Computation of propagative waves in free rail using a finite element technique," *J. Sound Vib.*, vol. 185, no. 3, pp. 531–543, 1995.

[21] A. T. I. Adamou and R. V. Craster, "Spectral methods for modelling guided waves in elastic media," *J. Acoust. Soc. Amer.*, vol. 116, no. 3, pp. 1524–1535, 2004.

[22] F. H. Quintanilla, M. J. S. Lowe, and R. V. Craster, "Modeling guided elastic waves in generally anisotropic media using a spectral collocation method," *J. Acoust. Soc. Amer.*, vol. 137, no. 3, pp. 1180–1194, 2015.

[23] M. Kaltenbacher, *Numerical Simulation of Mechatronic Sensors and Actuators: Finite Elements for Computational Multiphysics*, 3rd ed. New York, NY, USA: Springer, 2015.

[24] J. A. Weideman and S. C. Reddy, "A MATLAB differentiation matrix suite," *ACM Trans. Math. Softw.*, vol. 26, no. 4, pp. 465–519, 2000.

[25] D. Alleyne and P. Cawley, "A two-dimensional Fourier transform method for the measurement of propagating multimode signals," *J. Acoust. Soc. Amer.*, vol. 89, no. 3, pp. 1159–1168, May 1990.

[26] J. B. Harley and J. M. F. Moura, "Sparse recovery of the multimodal and dispersive characteristics of Lamb waves," *J. Acoust. Soc. Amer.*, vol. 133, no. 5, pp. 2732–2745, 2013.

[27] F. Schöpfer *et al.*, "Accurate determination of dispersion curves of guided waves in plates by applying the matrix pencil method to laser vibrometer measurement data," *CEAS Aeronaut. J.*, vol. 4, no. 1, pp. 61–68, 2013.

[28] S. J. Rupitsch, *Piezoelectric Sensors and Actuators: Fundamentals and Applications* (Topics in Mining, Metallurgy and Materials Engineering). Berlin, Germany: Springer, 2019.

[29] J. D. Achenbach, *Wave Propagation in Elastic Solids* (North-Holland Series in Applied Mathematics and Mechanics), 2nd ed. Amsterdam, The Netherlands: Elsevier, 1976.

[30] S. J. Rupitsch and J. Ilg, "Complete characterization of piezoceramic materials by means of two block-shaped test samples," *IEEE Trans. Ultrason., Ferroelectr., Freq. Control*, vol. 62, no. 7, pp. 1403–1413, Jul. 2015.

Michael Ponschab was born in Ingolstadt, Germany, in 1991. He received the M.Sc. degree in electrical engineering from Friedrich–Alexander Universität Erlangen–Nürnberg, Erlangen, Germany, in 2016, where he is currently pursuing the Ph.D. degree with the Department of Sensor Technology.

His research interests include ultrasonic sensing, elastodynamic guided waves, signal processing, and simulation-based material characterization.

Daniel A. Kiefer was born in Tumbaco-Quito, Ecuador, in 1989. He received the M.Sc. degree in mechatronics from Friedrich–Alexander Universität Erlangen–Nürnberg, Erlangen, Germany, in 2016, where he is currently pursuing the Ph.D. degree in ultrasonic sensing with the Department of Sensor Technology.

His research interests include guided elastodynamic waves, fluid–structure interaction and the corresponding numerical methods, and signal processing.

Stefan J. Rupitsch (S'07–M'09) was born in Kitzbuehel, Austria, in 1978. He received the Diploma and Ph.D. degrees in mechatronics from Johannes Kepler University, Linz, Austria, in 2004 and 2008, respectively, and the Habilitation degree from Friedrich–Alexander Universität Erlangen–Nürnberg, Erlangen, Germany, in 2018.

In 2004, he was a Junior Researcher with the Linz Center of Mechatronics, Linz. From 2005 to 2008, he was with the Institute for Measurement Technology, Johannes Kepler University. He is currently the Deputy Head of the Chair of Sensor Technology, Friedrich–Alexander Universität Erlangen–Nürnberg. His research interests include piezoelectric transducers and materials, simulation-based material characterization, ultrasonic imaging, and noncontacting measurements.

Dr. Rupitsch was a recipient of the Austrian Society of Measurement and Automation Technology Award for his Ph.D. dissertation in 2009 and the Outstanding Paper Award of the Information Technology Society in 2016. He is an Associate Editor of the IEEE SENSORS JOURNAL.

Authorized licensed use limited to: Universitatsbibliothek Erlangen Nurnberg. Downloaded on April 06,2020 at 09:45:45 UTC from IEEE Xplore. Restrictions apply.